Available online at www.sciencedirect.com

ScienceDirect

Ceramics International 40 (2014) 2973–2978

CERAMICS INTERNATIONAL

www.elsevier.com/locate/ceramint

Self-assembly synthesis of ZnO with adjustable morphologies and their photocatalytic performance

Yumin Liu*, Shuang Li, Hua Lv, Dan Ping, Shuangqing Li, Zijin Li, Haibo Tang

School of Chemistry and Chemical Engineering, Henan Normal University, Xinxiang 453007, Henan, PR China

Received 16 July 2013; received in revised form 2 October 2013; accepted 2 October 2013
Available online 11 October 2013

Abstract

ZnO with hierarchical microspheres and hexagonal prisms structures were successfully synthesized by hydrothermal microemulsion route. Based on X-ray diffraction and scanning electron microscopy observation of the products at the different reaction time periods, the formation mechanism of three-dimensional hierarchical ZnO microspheres was proposed. Ultraviolet and visible diffuse reflectance spectra indicated that as-synthesized ZnO microspheres had enhanced absorption in both ultraviolet and visible light areas. The photocatalytic activities of as-synthesized products were evaluated by monitoring the degradation of methylene blue solution. Due to the synergistic effects of the high crystallization and special hierarchical structure, the hierarchical ZnO microsphere exhibited the highest photocatalytic activity.

Keywords: D. ZnO; Mechanism; Hydrothermal microemulsion method; Microsphere

1. Introduction

In the past several decades, semiconductor-based photocatalyst has been widely used in wastewater treatment and air purification since Fujishima and Honda discovered the photocatalytic splitting of water on the TiO_2 electrodes in 1972 [1]. Among various oxide semiconductor photocatalysts, ZnO is recognized as an excellent material for photocatalytic processes and has been intensively investigated due to its high photosensitivity, nontoxic nature, large band gap and low cost [2,3]. Because of the strong correlation between the morphology, size, and structure of materials and their physical/chemical properties, much attention has been paid to design and prepare novel nano- and micro-structured materials [4]. Compared to mono-morphological structures, ZnO with three-dimensional (3D) complex hierarchical structures have been demonstrated to exhibit the enhanced photocatalytic performance [5]. Up to now, ZnO with 3D hierarchical structures have been successfully prepared *via* self-assembly based on different driving mechanisms. For examples, hierarchical flower-like C-doped ZnO superstructures assembled from porous nanosheets have been fabricated by pyrolysis of morphology-analogous $Zn_5(CO_3)_2(OH)_6$ precursors [6]. Liu et al., have synthesized spherical ZnO superstructures through a solvothermal method by adjusting synthetic parameters, i.e., synthetic basicity and temperature in the presence of surfactant molecules [7]. Self-assembly 3D porous ZnO nanostrip clusters have been prepared through a calcinating hydroxide zinc carbonate precursor route [8].

However, despite all these remarkable achievements, it still remains a great challenge for the controllable synthesis of hierarchically self-assembled architectures with desired size and morphology, especially by a simple and facile method. Among various synthetic strategies, the hydrothermal microemulsion method is a promising method for synthesizing ideal ZnO materials with special morphology. The main advantage of this method is low reaction temperature and short processing time that prevents agglomeration in the formed particles. In the present study, we report an efficient microemulsion-assisted hydrothermal method to synthesize ZnO hierarchical microspheres. The possible formation mechanism of the superstructures was put forward on the basis of a series of time-dependent experiments. Photocatalytic activity of the ZnO with different morphologies was evaluated through the degradation of methylene blue (MB). Moreover, the intensive relationship

*Corresponding author. Tel.: +86 373 332 6335; fax: +86 373 332 6336.
E-mail address: ymliu2007@163.com (Y. Liu).

0272-8842/$ - see front matter © 2013 Elsevier Ltd and Techna Group S.r.l. All rights reserved.
http://dx.doi.org/10.1016/j.ceramint.2013.10.011

between the microstructure and property of the obtained products was also discussed.

2. Experimental

2.1. Materials and synthesis

All of the reactants and solvents were analytical grade and used without any further purification. In a typical experimental procedure, two identical solutions were separately prepared by dissolving 2 g cetrimonium Bromide (CTAB) in 20 ml of cyclohexane and 4 ml of *n*-hexanol. Then, 2 ml of 0.5 M zinc acetate dihydrate and 2 ml of 0.25 M methenamine aqueous solutions were added to the two solutions, respectively. After vigorous stirring at room temperature for 30 min, the two optically transparent microemulsion solutions were mixed and stirred for another 30 min. The resulting microemulsion was transferred into a Teflon-lined stainless-steel autoclave and heated at 14 °C for appropriate time, followed by cooling to room temperature naturally. White products were separated by centrifugation and washed with deionized water and absolute ethanol several times. Then, the obtained ZnO samples were dried in vacuum at 50 °C for 12 h. The obtained ZnO samples were denoted as Sample-1, Sample-2, Sample-3, Sample-4 and Sample-5 when the reaction time was fixed for 1 h, 3 h, 6 h, 9 h and 14 h, respectively.

For comparison, ZnO with hexagonal prisms structures were synthesized using the same procedure mentioned above but the initial cosurfactant (*n*-hexanol) was replaced by *n*-butanol, while the other experimental conditions were kept unchanged [9]. The sample obtained for 14 h using *n*-butanol as cosurfactant was denoted as Sample-6.

2.2. Characterization

The crystal structure of the samples was determined by X-ray diffraction (Bruker D8 Advance, Germany) using graphite monochromated Cu Kα radiation ($\lambda = 0.15418$ nm) operated at 40 kV and 30 mA at a scan rate of 2 °/min. Morphologies of the samples were observed by scanning electron microscopy (JEOL JSM-63901, Japan) with an acceleration voltage of 25 kV. The Brunauer–Emmett–Teller (BET) surface area was determined, in terms of the N_2 adsorption on the power, using a volumetric adsorption apparatus (NOVA Surface Area Analyzer Station A, USA). Before the measurement, 0.1 g sample was outgassed under vacuum at 120 °C for 10 h. The BET surface area was determined by a multipoint BET method using the adsorption data in the relative pressure (P/P_0) range of 0.06–0.3. The pore size distribution was determined by the Barrett–Joyner–Halender (BJH) method using desorption branches. The optical absorption spectra of samples were recorded by ultraviolet and visible diffuse reflectance spectrophotometer (Cary5000 UV–vis–NIR) using $BaSO_4$ as a reference.

2.3. Photocatalytic test

The photocatalytic activities of as-prepared ZnO were evaluated by photocatalytic degradation of MB solution. All experiments were carried out in a photoreaction apparatus as reported in our previous study [10]. A 300 W high-pressure mercury lamp with the strongest emission at 365 nm was used as light source. In all experiments, 0.1 g of photocatalyst was added into 200 mL MB solution (50 mg L^{-1}). Before illumination, the suspension was sonicated for 10 min and stirred for 30 min in the dark to reach the adsorption–desorption equilibrium. At specific time intervals, 5 ml of the sample was withdrawn and centrifuged to separate the catalyst before analysis. For the determination of the MB concentration, ultraviolet and visible spectrophotometer was used at λ_{max} of 664 nm.

3. Results and discussion

3.1. Structure, morphology and growth mechanism

Fig. 1 shows the X-ray diffraction (XRD) patters of samples. All the diffraction peaks can be well indexed to the hexagonal wurtzite ZnO (JCPDS card no. 36-1451). No peaks of impurities can be observed indicating the high phase purity of as-synthesized samples. Moreover, it can be seen from Sample-1 to Sample-5 that the peak intensities steadily become stronger and the width of the diffraction peaks become slightly narrower with the prolonging of reaction time, indicating that extending of the reaction time can be beneficial for the formation and crystallization of ZnO microstructures. The average crystallite sizes (D) were determined from the XRD pattern using the Scherrer equation $D = 0.9\lambda/\beta \cos\theta$, where λ was the X-ray wavelength, β was the full width at half maximum (FWHM) of the diffraction line and θ was the diffraction angle. The values of β and θ were taken from ZnO (101) diffraction peak. The calculated crystallite sizes were 35,

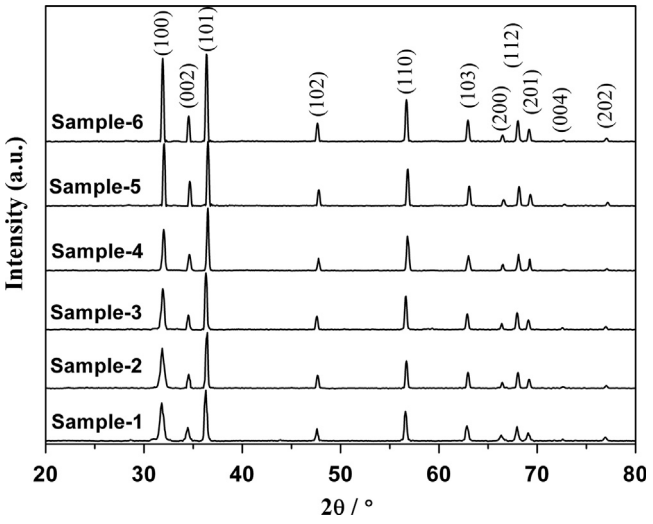

Fig. 1. XRD patterns of the samples.

40, 43, 48, 59, and 62 nm for the ZnO samples, referred to as Sample-1–Sample-6, correspondingly.

To understand the growth mechanism, samples prepared for different hydrothermal time were observed by scanning electron microscopy (SEM). As shown in Fig. 2A, in the initial stage (1 h), the resulting products were irregular plate-like structures. As the reaction was prolonged to 3 h (Fig. 2B), as-prepared ZnO samples were composed of uniform sheet-like architectures. As the reaction proceeded to 6 h (Fig. 2C), the flower-like ZnO structures consisted of many nanosheets were formed, but the superstructures were not very regular and uniform. After hydrothermal treatment of 9 h (Fig. 2D), more uniform flower-like structures were obtained. When the reaction time was prolonged to 14 h (Fig. 2E), the spaces among the intercrossed nanosheets of flower-like ZnO became compact and the shape of the obtained samples changed to 3D hierarchical microspheres. Clearly, as-synthesized ZnO microspheres hold three levels of structure. The primary structure is the layered crystal structure of ZnO. The secondary structure is the nanosheet assembled from nanoplates. The tertiary structure is the self-assembled spherical structure from as-formed nanosheets. Interestingly, ZnO with regularly hexagonal prisms structures (Fig. 2F) were obtained when *n*-butanol was used as the cosurfactant.

On the basis of the aforementioned SEM observation, the mechanism of spherical flower-like formation was proposed through three stages, namely anisotropic crystal growth, Ostwald ripening and self-assemble process. Initially, due to the decomposition of zinc acetate dihydrate and methenamine at an elevated temperature, the concentrations of Zn^{2+} and OH^- increases correspondingly. When the degree of supersaturation exceeds the critical value, ZnO nuclei start to form. With the increasing number of the ZnO nuclei, those nuclei begin to form small particles in the restricted water pools of the microemulsion system. Then, nanoplates were formed through the anisotropic growth of the small particles, which was related to both the anisotropic crystal structure of ZnO and the CTAB-involved solution conditions. The strong chelation reaction of CTAB ions with the growth units of $[Zn(OH)_4]^{2-}$ in the (001) plane might give rise to a suppression of crystal growth along the [001] axis and result in a relative enhancement of crystal growth along the [100]

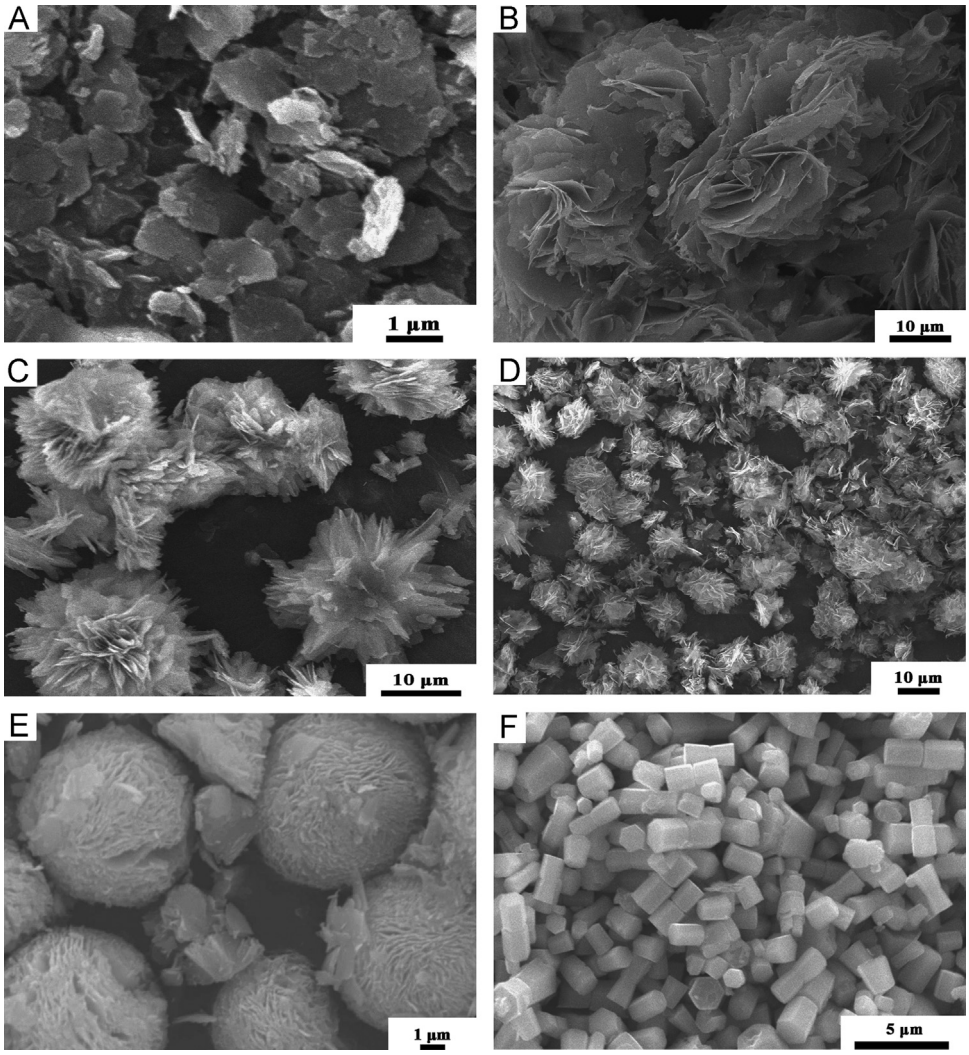

Fig. 2. SEM images of the samples: (A) Sample-1, (B) Sample-2, (C) Sample-3, (D) Sample-4, (E) Sample-5; and (F) Sample-6.

direction [11]. As a result, the growth of nanoplates in the presence of CTAB was more favorable. After 3 h reaction, further crystal growth would lead to the formation of nanosheets through the Ostwald ripening process, in which smaller particles disappeared due to their high solubility and crystallized to larger particles again. According to the thermodynamics point of view, the surface energy of an individual nanosheet was quite high because of its two main exposed planes, and thus they tended to aggregate to decrease the surface energy by reducing exposed areas. Because sphericity has the minimal surface energy, driven by the minimization of the interfacial energy, the formed nanosheets tend to self-organize along three-dimensional directions to form the spherical flower-like shape structures [12,13].

However, as shown in Fig. 2F, only hexagonal prisms were obtained when *n*-hexanol was replaced by *n*-butanol. As we know, the addition of cosurfactant has the influences on the curvature of micelles, surfactant aggregates and the surfactant film flexibility, which determines the growth of particles inside the reverse micelle and controls the morphology of the final nanocrystal [14–16]. It has been proven that the amount of alcohol acting as cosurfactant, which is located in the surfactant micelles, increases exponentially with the increase of alcohol's carbon chain length [17]. Due to the longer carbon chain than *n*-butanol, larger quantity of *n*-hexanol could locate in the surfactant micelles and decrease the surfactant film rigidity, which favors the anisotropic growth of ZnO crystals and consequently results in the formation of hierarchical structure [17,18]. When *n*-butanol was used as cosurfactant, the increasing rigidity of surfactant film and the decreasing steric hindrance might be beneficial for the orientated growth of ZnO crystals and regularly hexagonal prisms structures were formed finally. Obviously, more efforts should be paid to revealing the formation mechanism of the morphology controlled ZnO structures.

3.2. Physical properties

Ultraviolet and visible (UV–vis) diffuse reflectance spectra of as-prepared ZnO are shown in Fig. 3. It could be seen that absorption edges of all ZnO structures extended from the ultraviolet to visible light region. The absorption at wavelengths less than 400 nm can be assigned to the intrinsic band gap absorption of ZnO due to the electronic transitions from the valence to the conduction band ($O_{2p} \rightarrow Zn_{3d}$) [6]. This absorption in the visible region was attributed to the transition from the ground state to a few defect related deep states. Interestingly, Sample-5 exhibited an enhanced optical absorption both in the ultraviolet and visible light region. As reported by Zhang et al. [19], the shape and structure greatly affect the optical absorption and band-gap energy of semiconductors. The hierarchical organized structure of Sample-5 is beneficial for the enhanced light absorption due to multi-reflection of trapped incident light within the samples [20]. Therefore, the optical path length for light transport through the ZnO microspheres is longer, resulting in a greater absorption capacity.

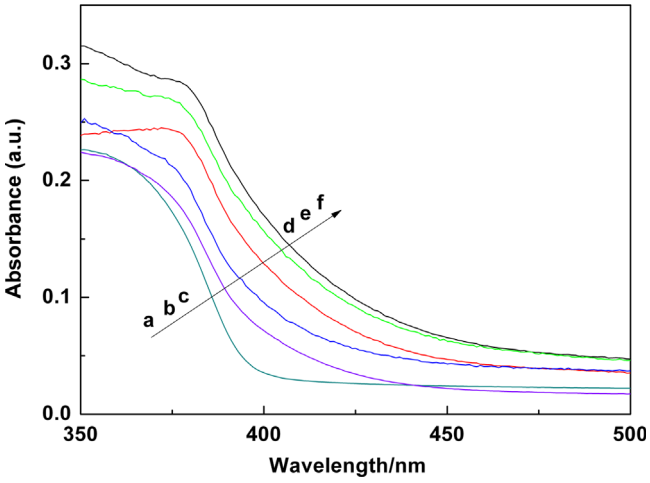

Fig. 3. UV–vis diffuse reflectance spectra of samples: (a) Sample-1, (b) Sample-2, (c) Sample-3, (d) Sample-6, (e) Sample-4, and (f) Sample-5.

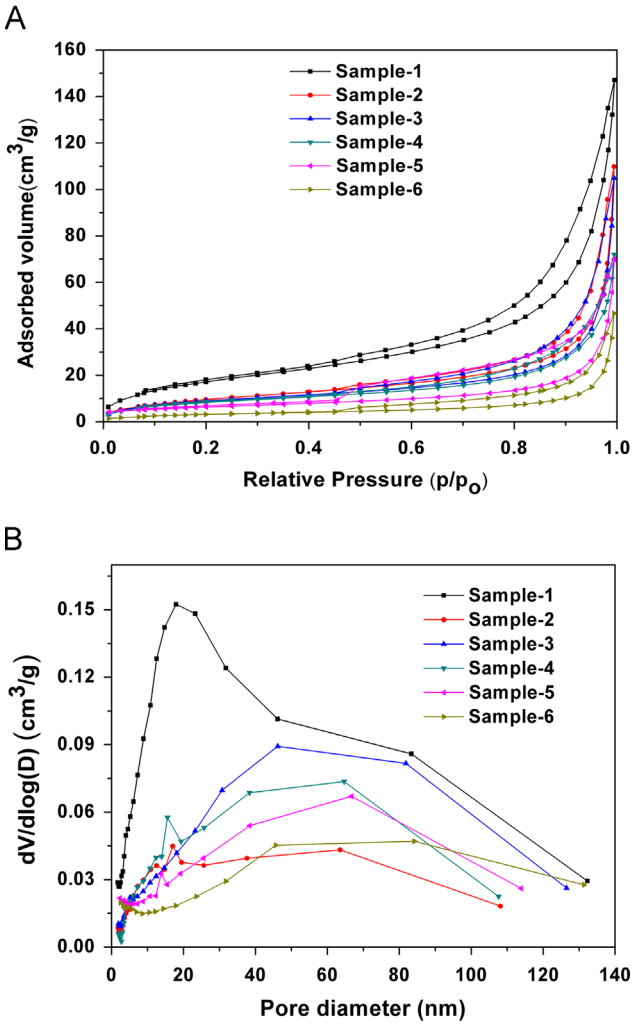

Fig. 4. N_2 adsorption/desorption isotherms (A) and pore size distribution plots and (B) of samples.

Fig. 4A shows the nitrogen adsorption/desorption isotherms of as-prepared ZnO. As shown in Fig. 4A, all isotherms can be categorized as type IV in the IUPAC classification with a

distinct hysteresis loop, which is characteristic of porous materials [21]. Moreover, the shape of the hysteresis loop is of type H3, indicating narrow slit-shaped pores that are generally associated with plate-like particles [6]. The porous structures of as-prepared samples are further confirmed by the corresponding pore-size distribution curves (Fig. 4B). As revealed by SEM observation, the smaller pores may be generated during the crystal growth process, while the larger pores are ascribed to the space between the intercrossed ZnO nanosheets [22]. As we know, the specific surface area strongly depends on the particle size. Generally, the surface area increases with the decreasing grain size. Based on BET calculation, the specific surface areas were 50.7, 25.6, 22.7, 20.1, 16.8 and 8.6 m^2/g for the ZnO samples, referred to as Sample-1-Sample-6, respectively, which is consistent with their increasing grain sizes.

3.3. Photocatalytic performance

The photocatalytic activities of ZnO synthesized with different morphologies were examined by photocatalytic degradation of MB under UV light irradiation. As shown in Fig. 5, ZnO with different morphologies exhibit large differences in activities and the photodegradation rates decrease in the following orders: Sample-5 > Sample-6 > Sample-4 > Sample-3 > Sample-2 > Sample-1. It is well known that the photocatalytic activity closely interrelates with the surface area, grain size, morphology, crystallization, the structure of photocatalyst, etc. Among them the surface area and crystallization are the important factors. Large specific surface area tends to expose more coordination unsaturated sites on the surface of catalyst, and more reactant can be absorbed onto the catalyst surface for reaction, leading to a higher photocatalytic activity [23]. Moreover, for randomly generated charge carriers, the average diffusion time from the bulk to the surface is given by $\tau = r^2/\pi^2 D$, where r is the grain radius and D is the diffusion coefficient of the carrier [24]. If the grain radius decreases, it will reduce the recombination opportunities of the photogenerated electron–hole pairs which could move effectively to the surface to degrade the absorbed MB molecules [25]. However, in our cases, ZnO with relatively higher surface areas and smaller grain size do not exhibit more impressive photocatalytic activities, which is not consistent with the common consideration. The possible explanation might be contributed to the crystallization, which is an another important factor influencing the photocatalytic activity [26]. A higher degree of crystallinity means fewer defects within the lattice and is beneficial for the transfer of photogenerated electron and holes. ZnO powders with large surface area are usually associated lower crystallization, which improve the recombination of photo-generated electrons and holes and result in the poor photocatalytic activity [27,28]. Therefore, due to the lower crystallization, ZnO powders (Sample-1–Sample-4) with relatively higher surface area exhibited the poor photocatalytic activity. Another important reason for the high photocatalytic activity of Sample-5 should be attributed to the novel 3D hierarchical microspheres superstructures. As shown in Fig. 2E, many pores with different diameter sizes can be found among the nanoplates in the hierarchical structures of Sample-5, which may serve as transport paths for small molecules and consequently improve the photocatalytic properties. Moreover, as shown in Fig. 3, the 3D hierarchical structure of Sample-5 can enhance light harvesting and utilize the light source more efficiently, which thus offers an improved catalytic activity [20]. Therefore, the enhanced photocatalytic activity of Sample-5 might be attributed to the synergistic consequence of the high crystallization and special 3D hierarchical structure.

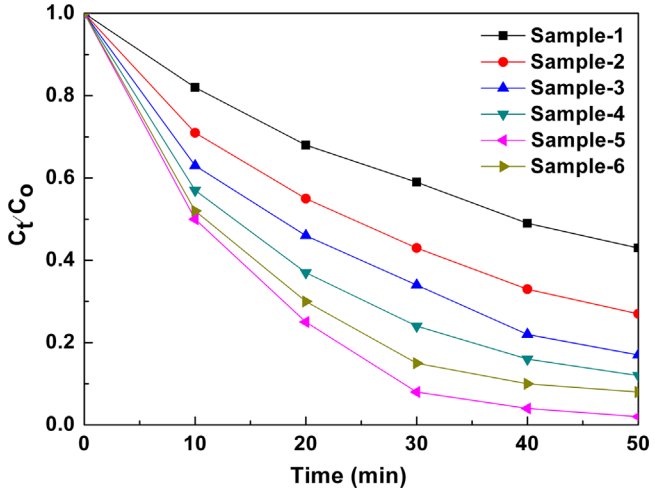

Fig. 5. Photocatalytic degradation of MB by ZnO samples.

4. Conclusions

In summary, regularly 3D hierarchical ZnO microspheres built from 2D nanosheets alignment have been successfully obtained by hydrothermal microemulsion route. Various morphologies of the ZnO, i.e., sheet-like, flower-like, microspheres and hexagonal prisms, can be controlled by simply changing the reaction time and the types of cosurfactants. Based on a series of time-dependent experiments, the plausible formation mechanism for the hierarchical ZnO microspheres was proposed. The possible explanation for the highest activity of hierarchical ZnO microspheres might be attributed to the synergistic consequence of the high crystallization and special 3D hierarchical structure.

Acknowledgments

The authors gratefully acknowledge the financial support from the National Natural Science Foundation of China (Grant no. U1204503) and the Youth Backbone Teachers Supporting Plan Project of Henan Normal University (Grant no. 01036500610).

References

[1] A. Fujishima, K. Honda, Electrochemical photolysis of water at a semiconductor electrode, Nature 238 (5358) (1972) 37–38.
[2] H.R. Pant, B. Pant, R.K. Sharma, A. Amarjargal, H.J. Kim, C.H. Park, L.D. Tijing, C.S. Kim, Antibacterial and photocatalytic properties of

Ag/TiO_2/ZnO nano-flowers prepared by facile one-pot hydrothermal process, Ceram. Int. 39 (2) (2013) 1503–1510.
[3] Y.-X. Wang, J. Sun, X. Fan, X. Yu, A CTAB-assisted hydrothermal and solvothermal synthesis of ZnO nanopowders, Ceram. Int. 37 (8) (2011) 3431–3436.
[4] M. Shang, W. Wang, H. Xu, New Bi_2WO_6 Nanocages with High Visible-Light-Driven Photocatalytic Activities Prepared in Refluxing EG, Cryst. Growth Des. 9 (2) (2008) 991–996.
[5] H. Sun, Y. Yu, J. Luo, M. Ahmad, J. Zhu, Morphology-controlled synthesis of ZnO 3D hierarchical structures and their photocatalytic performance, Cryst. Eng. Commun. 14 (24) (2012) 8626–8632.
[6] S. Liu, C. Li, J. Yu, Q. Xiang, Improved visible-light photocatalytic activity of porous carbon self-doped ZnO nanosheet-assembled flowers, Cryst. Eng. Commun. 13 (7) (2011) 2533–2541.
[7] L. Liu, M. Ge, H. Liu, C. Guo, Y. Wang, Z. Zhou, Controlled synthesis of ZnO with adjustable morphologies from nanosheets to microspheres, Colloid Surf. A 348 (1–3) (2009) 124–129.
[8] Z. Xing, B. Geng, X. Li, H. Jiang, C. Feng, T. Ge, Self-assembly fabrication of 3D porous quasi-flower-like ZnO nanostrip clusters for photodegradation of an organic dye with high performance, Cryst. Eng. Commun. 13 (6) (2011) 2137–2142.
[9] Y. Liu, H. Lv, S. Li, X. Xing, G. Xi, Preparation and photocatalytic property of hexagonal cylinder-like bipods ZnO microcrystal photocatalyst, Dyes Pigm. 95 (3) (2012) 443–449.
[10] Y. Liu, L. Hua, S. Li, Photocatalytic degradation of reactive brilliant blue KN-R by TiO_2/UV process, Desalination 258 (1–3) (2010) 48–53.
[11] Z. Li, Y. Fang, L. Peng, D. Pan, M. Wu, EDTA-assisted synthesis of rose-like ZnO architectures, Cryst. Res. Technol. 45 (10) (2010) 1083–1086.
[12] W. Zhao, X. Song, Z. Yin, C. Fan, G. Chen, S. Sun, Self-assembly of ZnO nanosheets into nanoflowers at room temperature, Mater. Res. Bull. 43 (11) (2008) 3171–3176.
[13] J. Wu, F. Duan, Y. Zheng, Y. Xie, Synthesis of Bi_2WO_6 nanoplate-built hierarchical nest-like structures with visible-light-induced photocatalytic ACTIVITY, J. Phys. Chem. C 111 (34) (2007) 12866–12871.
[14] W. Fan, X. Song, S. Sun, X. Zhao, Microemulsion-mediated hydrothermal synthesis and characterization of zircon-type $LaVO_4$ nanowires, J. Solid State Chem. 180 (1) (2007) 284–290.
[15] M.L. Curri, A. Agostiano, L. Manna, M.D. Monica, M. Catalano, L. Chiavarone, V. Spagnolo, M. Lugarà, Synthesis and characterization of CdS nanoclusters in a quaternary microemulsion: the role of the cosurfactant, J. Phys. Chem. B 104 (35) (2000) 8391–8397.
[16] P. Ågren, M. Lindén, J.B. Rosenholm, R. Schwarzenbacher, M. Kriechbaum, H. Amenitsch, P. Laggner, J. Blanchard, F. Schüth, Kinetics of cosurfactant – surfactant – silicate phase behavior. 1. short-chain alcohols, J. Phys. Chem. B 103 (29) (1999) 5943–5948.
[17] W.-Q. Wang, J.-G. Wang, P.-C. Sun, D.-T. Ding, T.-H. Chen, Effect of alcohol on morphology and mesostructure control of anionic-surfactant-templated mesoporous silica AMS, J. Colloid Interface Sci. 331 (1) (2009) 156–162.
[18] R. Ranjan, S. Vaidya, P. Thaplyal, M. Qamar, J. Ahmed, A.K. Ganguli, Controlling the Size, Morphology, and Aspect Ratio of Nanostructures Using Reverse Micelles: A Case Study of Copper Oxalate Monohydrate, Langmuir 25 (11) (2009) 6469-6475.
[19] H. Huang, H. Chen, Y. Xia, X. Tao, Y. Gan, X. Weng, W. Zhang, Controllable synthesis and visible-light-responsive photocatalytic activity of Bi_2WO_6 fluffy microsphere with hierarchical architecture, J. Colloid Interface Sci. 370 (1) (2012) 132–138.
[20] H. Li, Z. Bian, J. Zhu, D. Zhang, G. Li, Y. Huo, H. Li, Y. Lu, Mesoporous titania spheres with tunable chamber stucture and enhanced photocatalytic activity, J. Am. Chem. Soc. 129 (27) (2007) 8406–8407.
[21] S. Liu, J. Yu, Cooperative self-construction and enhanced optical absorption of nanoplates-assembled hierarchical Bi_2WO_6 flowers, J. Solid State Chem. 181 (5) (2008) 1048–1055.
[22] Y. Li, J. Liu, X. Huang, G. Li, Hydrothermal synthesis of Bi_2WO_6 uniform hierarchical microspheres, Cryst. Growth Des. 7 (7) (2007) 1350–1355.
[23] T.L. Thompson, J.T. Yates Jr., Surface science studies of the photoactivation of TiO_2-new photochemical processes, Chem. Rev. 106 (10) (2006) 4428–4453.
[24] J.W. Tang, Z.G. Zou, J.H. Ye, Efficient photocatalytic decomposition of organic contaminants over $CaBi_2O_4$ under visible-light irradiation, Angew. Chem. Int. Ed. 43 (34) (2004) 4463–4466.
[25] Y. Mi, S. Zeng, L. Li, Q. Zhang, S. Wang, C. Liu, D. Sun, Solvent directed fabrication of Bi_2WO_6 nanostructures with different morphologies: synthesis and their shape-dependent photocatalytic properties, Mater. Res. Bull. 47 (9) (2012) 2623–2630.
[26] J. Yu, W. Wang, B. Cheng, B. Huang, X. Zhang, Preparation and photocatalytic activity of multi-modally macro/mesoporous titania, Res. Chem. Intermed. 35 (6-7) (2009) 653–665.
[27] J. Yu, G. Wang, B. Cheng, M. Zhou, Effects of hydrothermal temperature and time on the photocatalytic activity and microstructures of bimodal mesoporous TiO_2 powders, Appl. Catal. B 69 (3–4) (2007) 171–180.
[28] J. Yu, S. Liu, M. Zhou, Enhanced photocalytic activity of hollow anatase microspheres by Sn^{4+} incorporation, J. Phys. Chem. C 112 (6) (2008) 2050–2057.